Available online at www.sciencedirect.com
ScienceDirect
International Journal of Heat and Mass Transfer 51 (2008) 3245–3250
International Journal of HEAT and MASS TRANSFER
www.elsevier.com/locate/ijhmt

Technical Note

A boundary layer analysis for entrance region heat transfer in vertical microchannels within the slip flow regime

Suman Chakraborty *, S.K. Som, Rahul

Department of Mechanical Engineering, Indian Institute of Technology, Kharagpur 721302, India

Received 19 September 2007; received in revised form 7 January 2008
Available online 24 March 2008

Abstract

A boundary layer integral analysis has been executed to investigate the heat transfer characteristics of natural convection gas flows in symmetrically heated vertical microchannels, under the conditions of large channel aspect ratios, in the slip flow regime. It has been revealed that for low values of Rayleigh number, the entrance region length is only a small fraction of the total channel extent. For higher values of Rayleigh number, however, effects of the developing region are non-trivial, and two counteracting heat transfer mechanisms need to be aptly taken into consideration for interpreting the Nusselt number values. In the present study, the proportionate enhancement in the average Nusselt number with wall-slip effects has been observed to become more prominent for higher values of Knudsen number. However, the relative augmentation in the rate of heat transfer tends to get somewhat arrested for higher values of Rayleigh number, as attributable to the counteracting influences of augmented rates of advective transport and reduced wall-adjacent temperature gradients. For all cases, the boundary layer theory based predictions have been found to agree excellently with the corresponding results obtained from full-scale numerical predictions.

1. Introduction

Microelectromechanical systems (MEMS) based devices find their applications in a wide variety of emerging technologies, ranging from microactuators, microsensors, microreactors to thermo-mechanical data storage systems, to name a few. Design and optimization of many of these microdevices involve the analysis of gas flows through microchannels, thereby emphasizing the need for reliable analytical capabilities to address the pertinent issues that are closely associated with the fundamentals of thermo-fluidic transport of gases over reduced length scales [1].

The primary challenges associated with the mathematical analysis of microscale gaseous flows originate from the fact that the flow physics tend to get changed altogether, as one reduces the length scales from the macro domain to the micro domain. The classical continuum hypothesis ceases to work as the distance traversed by molecules between successive collisions (i.e., the mean free path, λ) becomes comparable with the characteristic length scale of the system (L) over which characteristic changes in the transport phenomena are expected to occur. The ratio of these two quantities, known as the Knudsen number ($Kn = \lambda/L$), is an indicator of the degree of rarefaction of the system, which determines the extent of deviation from a possible continuum behaviour. For $0 < Kn < 0.01$, the flow domain can be treated as a continuum, in which the Navier Stokes equation in conjunction with the no-slip wall boundary conditions become applicable. On the other extreme, when $Kn > 10$, the flow becomes free molecular in nature, because of negligible molecular collisions. The range of Kn spanning from 0.01 to 0.1 is known as the slip flow regime, over which the no-slip boundary condition becomes invalid, although continuum conservation equations can still be used to characterize the bulk flow. This regime of flow has perhaps attracted most serious attention

* Corresponding author. Tel.: +91 3222 282990; fax: +91 3222 282278.
E-mail address: suman@mech.iitkgp.ernet.in (S. Chakraborty).

0017-9310/$ - see front matter © 2008 Published by Elsevier Ltd.
doi:10.1016/j.ijheatmasstransfer.2008.01.019

from the engineering research community till date, because of its immense significance associated with many of the practical and technologically important microfluidic devices [1].

Convective transport in microchannels over the slip flow regime has been the focal point of attention of many research studies in the recent past. However, despite a wide-ranging technological importance of natural convection in microchannels, only a few studies reported in the literature have aptly emphasized on the underlying scientific issues. Chen and Weng [2] recently presented analytical investigations on fully developed natural convection in open–ended vertical parallel plate microchannels, by taking the velocity slip and temperature jump effects into account. An important conclusion from their study is that for fully developed free convection flows with symmetrically heated walls, the Nusselt number turns out to be zero. These conclusions, however, were made by neglecting the momentum and heat transfer characteristics in the developing region of the microchannel. Appreciating the fact that the transport phenomena in the developing region might influence the characteristics of the fully developed natural convection in vertical microchannels in a rather profound manner, Biswal et al. [3] have recently executed a comprehensive computational study on free convection heat transfer in the entrance region, followed by that in the fully developed region, in long vertical microchannels, for different values of Knudsen number and Rayleigh number. In their study, special implications of accommodating the effects of the developing region in the heat transfer analysis were discussed in details and some important conclusions based on the same were pinpointed. Haddad et al. [4] have reported implicit finite difference simulations of the developing natural convection in an isothermally heated microchannel filled with porous media. Chen and Weng [5], in a subsequent study, have emphasized the importance of thermal creep and high order slip/jump conditions for modeling developing natural convection problems, by employing a marching implicit procedure.

Despite the fact that detailed computational studies have been reported in the literature on the entrance region free convection transport in vertical microchannels, it is important to appreciate that such full-scale numerical simulation studies often demand computationally expensive efforts for solving practical design problems for wide parametric variations in the operating conditions. In that respect, boundary layer based semi-analytical methodologies might not only turn out to be computationally much less demanding, but also are likely to provide direct physical insights regarding the fundamental physics of transport phenomena in the entrance region in a more elegant manner. Not only that, numerous parametric variations can be studied with the help of such analysis, without incurring stringent computational constraints. Having said that, it is also important to appreciate that such formalism is by no means trivial to establish, primarily attributed to the velocity slip and temperature jump effects occurring at the wall-fluid interface.

Aim of the present work, accordingly, is to develop a boundary layer based model on free convection heat transfer in vertical microchannels, with a primary vision of capturing the interplay between the boundary layer growth in the developing region and the microscale effects manifested through wall-slippage and temperature jump conditions at the gas–solid interface. To the best of our knowledge, such analysis is yet to be comprehensively executed in the context of free convective heat transfer in vertical microchannels. The outcome of the present analysis is also compared with the corresponding predictions obtained from full-scale numerical simulations, so as to make a rational assessment on the predictive capabilities of the present semi-analytical approach.

2. Mathematical modeling

For mathematical modeling, we consider a vertical parallel plate microchannel with the coordinate system and other geometrical details as shown in the Fig. 1. The length (L) of the channel is considered to be much larger than the width (H). The flow is considered to be two-dimensional. The temperature of the channel walls is uniform at T_w. The channel is open at both the ends to the ambient with temperature of T_∞, which is lower than T_w. This temperature difference generates an upward buoyancy induced flow in the microchannel. The physical properties of the gas are assumed to be constant (comparisons with variable-property based full-scale numerical simulation predictions are resented later for justifying this assumption). The compressibility effects and viscous heat dissipation are neglected [6] due to the assumption of low speed micro flow (Mach number less than 0.3).

The governing continuity, momentum and energy equations for steady, incompressible and laminar flow in the microchannel are as follows:

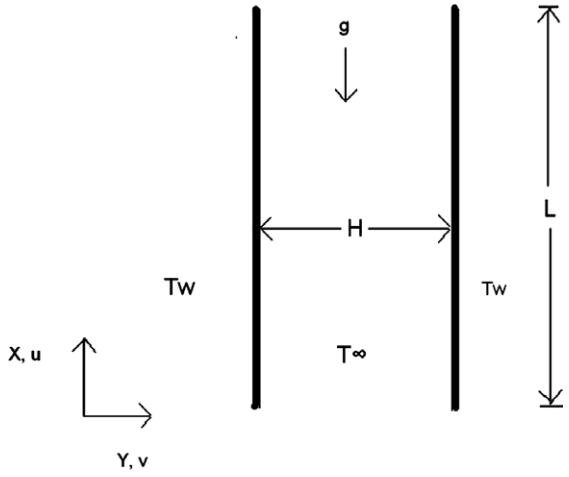

Fig. 1. A schematic showing the problem geometry along with the coordinate system adopted.

$$\text{Continuity equation}: \frac{\partial u}{\partial x}+\frac{\partial v}{\partial y}=0 \tag{1}$$

X-momentum equation :

$$\rho\left(u\frac{\partial u}{\partial x}+v\frac{\partial u}{\partial y}\right)=-\frac{\partial p}{\partial x}-\rho g+\mu\left(\frac{\partial^2 u}{\partial x^2}+\frac{\partial^2 u}{\partial y^2}\right) \tag{2}$$

Y-momentum equation :

$$\rho\left(u\frac{\partial v}{\partial x}+v\frac{\partial v}{\partial y}\right)=-\frac{\partial p}{\partial y}+\mu\left(\frac{\partial^2 v}{\partial x^2}+\frac{\partial^2 v}{\partial y^2}\right) \tag{3}$$

$$\text{Energy equation}: \rho C_{\mathrm{p}}\left(u\frac{\partial T}{\partial x}+v\frac{\partial T}{\partial y}\right)=k\left(\frac{\partial^2 T}{\partial x^2}+\frac{\partial^2 T}{\partial y^2}\right) \tag{4}$$

For executing a boundary layer analysis, the following scales are considered: $u\sim U$, $v\sim V$, $x\sim L$, $y\sim\delta$, such that $\frac{\delta}{L}\ll 1$. Invoking the Boussinesq approximation, the boundary layer equations for momentum and energy conservation are written as

$$u\frac{\partial u}{\partial x}+v\frac{\partial u}{\partial y}=g\beta(T-T_\infty)+v\frac{\partial^2 u}{\partial y^2} \tag{5}$$

$$u\frac{\partial T}{\partial x}+v\frac{\partial T}{\partial y}=\alpha\frac{\partial^2 T}{\partial y^2} \tag{6}$$

where v is the kinematic viscosity, α is the thermal diffusivity, and $\beta=-\frac{1}{\rho}\frac{\partial\rho}{\partial T}=\frac{\rho_\infty-\rho}{\rho(T-T_\infty)}$ is the volumetric expansion coefficient.

The momentum and the energy equations can be integrated over the respective boundary layers to obtain the following integral forms:

$$\frac{\mathrm{d}}{\mathrm{d}x}\left(\int_0^\delta u^2\mathrm{d}y\right)=-v\left(\frac{\partial u}{\partial y}\right)_{y=0}+\int_0^\delta \beta g(T-T_\infty)\mathrm{d}y \tag{7}$$

$$\frac{\mathrm{d}}{\mathrm{d}x}\left(\int_0^{\delta_t} u(T-T_\infty)\mathrm{d}y\right)=-\alpha\left(\frac{\partial T}{\partial y}\right)_{y=0} \tag{8}$$

where δ and δ_{t} are the local hydrodynamic and thermal boundary layer thicknesses, respectively, at any given axial location x. Defining $\eta_{\mathrm{t}}=\frac{y}{\delta_{\mathrm{t}}}$, the following temperature profile may be assumed within the thermal boundary layer:

$$\frac{T-T_\infty}{T_{\mathrm{w}}-T_\infty}=\frac{1}{1+2A\left(\frac{H}{\delta_{\mathrm{t}}}\right)}\left(1-\frac{y}{\delta_{\mathrm{t}}}\right)^2 \tag{9}$$

(i) At $y=\delta_{\mathrm{t}}$, $T=T_\infty$
(ii) At $y=\delta_{\mathrm{t}}$, $\frac{\partial T}{\partial y}=0$
(iii) At $y=0$, $T-T_{\mathrm{w}}=\frac{2-\sigma_T}{\sigma_T}\left[\frac{2\gamma}{\gamma+1}\right]\frac{Kn}{Pr}\left\{\frac{\partial T}{\partial(y/H)}\right\}$

Analogously, the velocity profile is taken as

$$\frac{u}{u_x}=\frac{1}{\left(3B\frac{H}{\delta}+2\right)}\left[\left\{\left(\frac{y}{\delta}\right)-2\left(\frac{y}{\delta}\right)^2+\left(\frac{y}{\delta}\right)^3\right\}+B\frac{H}{\delta}\left\{1-3\left(\frac{y}{\delta}\right)^2+2\left(\frac{y}{\delta}\right)^3\right\}\right] \tag{10}$$

where $B=\frac{2-\sigma_v}{\sigma_v}Kn$, and $u_x=\frac{g\beta(T_{\mathrm{w}}-T_\infty)\delta^2}{2v}$. The above velocity profile is obtained by satisfying the following boundary conditions:

(i) At $y=\delta$, $u=0$
(ii) At $y=\delta$, $\frac{\partial u}{\partial y}=0$
(iii) At $y=0$, $\frac{\partial^2 u}{\partial y^2}=-\frac{g\beta}{v}(T_{\mathrm{w}}-T_\infty)$
(iv) At $y=0$, $u=\frac{2-\sigma_v}{\sigma_v}Kn\frac{\partial u}{\partial(y/H)}$

For the convenience of obtaining semi-analytical solutions, the Prandtl number is assumed to be close to unity, so that $\delta\sim\delta_{\mathrm{t}}$. For that case, the profiles given by Eqs. (9) and (10) are substituted in Eqs. (7) and (8), to yield:

$$\frac{1}{105}\frac{\mathrm{d}}{\mathrm{d}x}\left[\frac{u_x^2\delta\left\{1+11B\frac{H}{\delta}+39B^2\left(\frac{H}{\delta}\right)^2\right\}}{\left(3B\frac{H}{\delta}+2\right)^2}\right]=-\frac{vu_x}{\delta\left(3B\frac{H}{\delta}+2\right)}+\frac{\delta\beta g(T_{\mathrm{w}}-T_\infty)}{3\left(1+2A\frac{H}{\delta}\right)} \tag{11}$$

$$\frac{1}{30}\frac{\mathrm{d}}{\mathrm{d}x}\left[\frac{u_x\delta\left(1+8B\frac{H}{\delta}\right)}{\left(1+2A\frac{H}{\delta}\right)\left(3B\frac{H}{\delta}+2\right)}\right]=\frac{2\alpha}{\delta\left(1+2A\frac{H}{\delta}\right)} \tag{12}$$

It is interesting to note here that the above equations represent the special cases of no-slip and no temperature jump conditions at the wall, on setting A, $B=0$, so that classical equations pertaining to the boundary layer analysis of macro-scale free convective transport [7] can be recovered as a special case of the present analysis. For the more general case considered in this study, u_x can be eliminated from Eqs. (11) and (12) to yield:

$$\frac{\mathrm{d}\Delta^4}{\mathrm{d}X}=\frac{16a}{Ra}\left[60-\left(\frac{35}{2}\right)Pr\frac{\Delta(\Delta+8B)\{\Delta+6(B-A))\}}{(\Delta+2A)(\Delta^2+11B\Delta+39B^2)}\right]\frac{(3B+2\Delta)^2}{(\Delta+8B)}\times\left[\frac{4\{\Delta^3+(11B+4A)\Delta^2+(17AB+12B^2)\Delta+48AB^2\}}{(\Delta+2A)(\Delta+8B)}-\frac{(2\Delta^3+9B\Delta^2-12B^2\Delta+117B^3)}{(\Delta^2+11B\Delta+39B^2)}\right]^{-1} \tag{13}$$

where $A=\frac{2-\sigma_T}{\sigma_T}\left[\frac{2\gamma}{\gamma+1}\right]\frac{Kn}{Pr}$. Here $Kn=\frac{\mu}{H\rho(2RT_{\mathrm{w}}/\pi)^{1/2}}$ and $Pr=\frac{\mu C_{\mathrm{p}}}{k}$. The above temperature profile is constrained to satisfy the following boundary conditions:

where $Ra=\frac{g\beta(T_{\mathrm{w}}-T_\infty)H^3}{v\alpha}$, $\Delta=\left(\frac{\delta}{H}\right)$ and $X=\frac{x}{H}$. Eq. (13) can be cast in the following form:

$$\frac{dZ}{dX} = f(Z) \tag{14}$$

where $Z = \Delta^4$, and the function f is given by

$$f(Z) = \frac{16a}{Ra}\left[60 - \left(\frac{35}{2}\right)Pr\frac{Z^{1/4}(Z^{1/4}+8B)\{Z^{1/4}+6(B-A)\}}{(Z^{1/4}+2A)(Z^{1/2}+11BZ^{1/4}+39B^2)}\right]\frac{(3B+2Z^{1/4})^2}{(Z^{1/4}+8B)} \times \left[\frac{4\{Z^{3/4}+(11B+4A)Z^{1/2}+(17AB+12B^2)Z^{1/4}+48AB^2\}}{(Z^{1/4}+2A)(Z^{1/4}+8B)} - \frac{(2Z^{3/4}+9BZ^{1/2}-12B^2Z^{1/4}+117B^3)}{(Z^{1/2}+11BZ^{1/4}+39B^2)}\right]^{-1} \tag{15}$$

Eq. (14) is solved using the fourth order Runge Kutta method [3], to obtain the evolution of the boundary layer as a function of the axial coordinate, X. The results are parameterized in terms of the parameters A and B and Ra (as appearing in Eq. (15)), or equivalently in terms of Ra and Kn, with $Pr = 1$. Further, diffuse reflections with full accommodation ($\sigma_v = 1$, $\sigma_T = 1$) are considered for velocity slip and temperature jump boundary conditions. The local Nusselt number is calculated as

$$Nu = \frac{-\left(\frac{\partial T}{\partial x}\right)_w H}{(T_w - T_\infty)} \tag{16}$$

3. Results and discussion

In order to compare the present numerical solutions with the results obtained from full-scale numerical computations, the variation of the non-dimensional entrance length with Rayleigh number (Ra), for different values of Knudsen number (Kn), are compared with those obtained by Biswal et al. [3], as shown in the Fig. 2. A very good agreement can be obtained in this regard. It is evident from the figure that a higher value of Ra results in a longer entrance region. In fact, for lower values of Rayleigh number, the entrance length is negligible and the flow can be assumed to be completely fully developed over the entire channel length. Moreover, the entrance length also increases with enhancements in the value of Kn. This can be attributed to the fact that for a given temperature differential between the wall and the bulk stream, the velocity slip and temperature jump conditions at the walls give rise to higher flow velocities. Higher the value of Kn, more prominent is this effect. This effectively decreases the near wall velocity and temperature gradients and retards the growth of both hydrodynamic and thermal boundary layers, so that the entrance length is effectively increased.

Fig. 3 depicts the variation in the local Nusselt number (Nu), along the microchannel height, for different values of Kn. These variations are characterized with an initial steep fall in Nu, followed by an asymptotic decrement towards zero in the fully developed region. It is primarily a rapid growth of the thermal boundary layer in microchannel flows that gives rise to the steep initial gradients. However, with higher values of Kn, the boundary layer growth is somewhat delayed, as explained earlier. This leads to a delayed attainment of the thermally fully developed state. From Fig. 3 it is also apparent that the predictions from boundary layer theory agree quite well with the predictions made from full-scale numerical simulations.

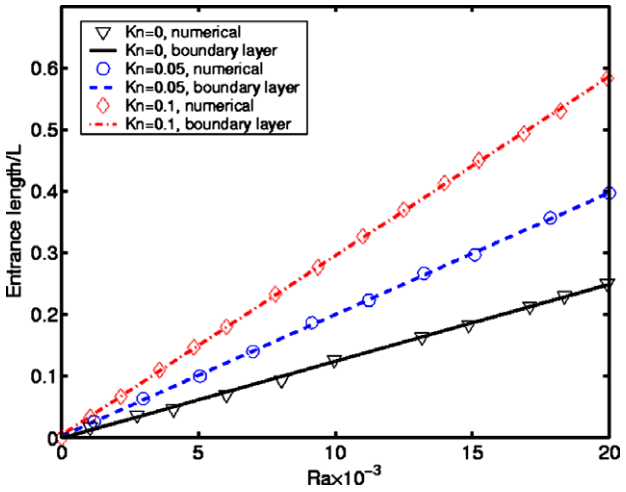

Fig. 2. Variation of non-dimensional entrance length with Rayleigh number for different values Knudsen number: comparison between boundary layer solution and full-scale numerical solution [3]. L/H is taken as 10^5 for the calculations.

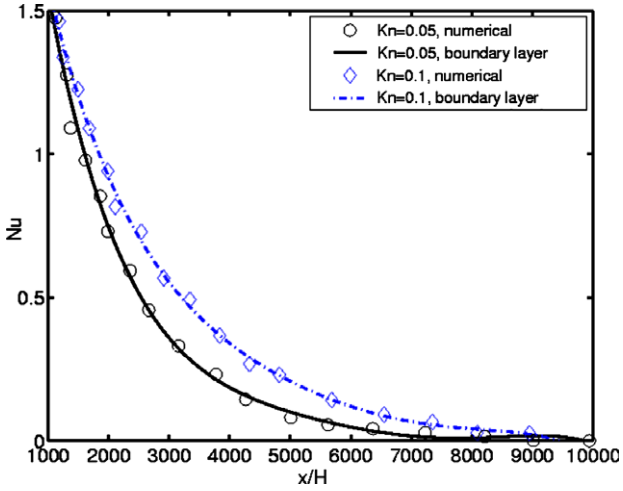

Fig. 3. Variations in local Nusselt number along the height of channel, for $Ra = 10^5$, with different values of Kn: comparison between boundary layer solution and full-scale numerical solution [3].

Fig. 4 depicts the variations of the axially-averaged *Nu* with *Ra*, for different values of *Kn*. For low values of *Ra*, the average *Nu* approaches zero. This is attributable to the fact that for such cases the flow becomes fully developed after traversing a very short distance, on entering the channel. However, the extent of the entrance region becomes significantly more prominent as the Rayleigh number increases. Further, with higher values of *Kn*, the entrance region transport is more emphatically dictated by the wall-slip effects. For a given imposed pressure gradient on account of thermal buoyancy effects, the mass flow rate tends to increase significantly with more prominent wall-slippage effects, leading to an enhancement in the rate of heat transfer. On the other hand, a higher value of *Kn* also implies more significant temperature jump at the walls, which tends to decrease the driving temperature gradient for convective heat transfer between the wall-adjacent layer and the bulk fluid. Although this effect counterbalances the effect of augmented advective transport to some extent, it is found to be insufficient in totally overweighing the influences of the later, so that an augmentation in the average rate of heat transfer with increments in the value of *Kn* occurs for the cases represented in Fig. 4. However, the relative augmentation in the rate of heat transfer tends to get arrested to some extent for higher values of *Ra*. This can be attributed to the counteracting influences of augmented advective transport and reduced wall-adjacent temperature gradients. With regard to the prediction of average Nusselt number for the cases investigated, there appears to be an excellent agreement between the boundary layer solutions and full-scale numerical predictions [3].

The semi-analytical method that has been developed here can elegantly be employed to capture the thermal creep effects in the wall-slip boundary conditions, with possible higher order extensions. As a first extension towards accommodating thermal creep effects at the wall, following additional term is considered for the pertinent velocity

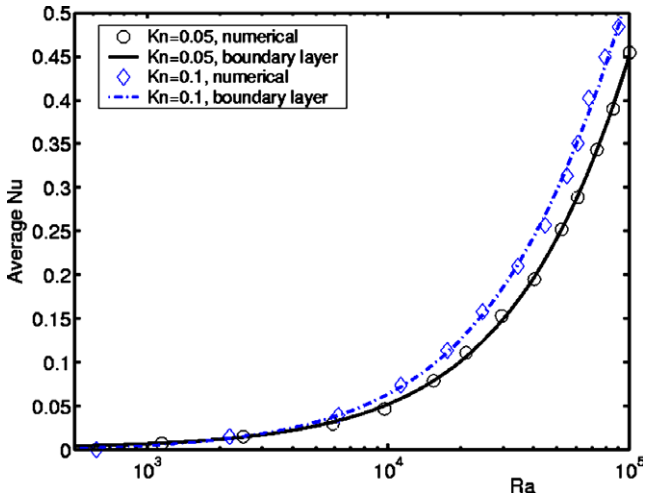

Fig. 4. Variations in average Nusselt number with Rayleigh number for different values of *Kn*: comparison between boundary layer solution and full-scale numerical solution [3].

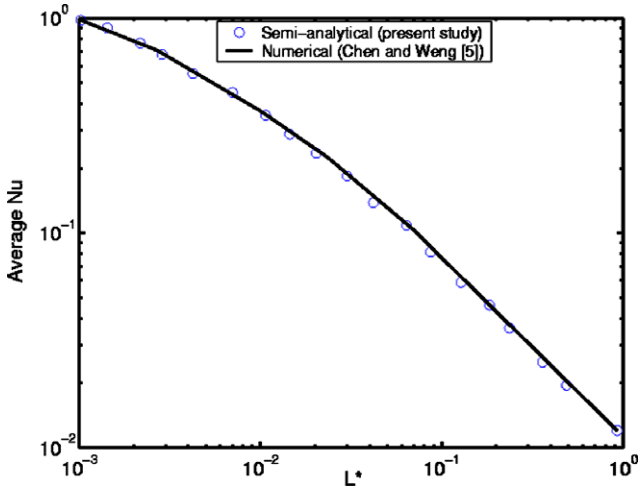

Fig. 5. Variations in average Nusselt number with non-dimensional channel height for $Kn = 0.09$: comparison between the present solution and numerical solution [5].

boundary condition: $u_{\text{add}} = \frac{3}{2\pi}\frac{\gamma-1}{\gamma}\frac{\rho_\infty C_p}{\mu}\lambda^2\frac{\partial T}{\partial x}\big|_{\text{wall}}$. The first order wall-jump conditions are subsequently augmented to higher order effects by replacing the molecular mean free path with [5] $l_c\lambda/(l_c - b\lambda)$, where l_c is the characteristic length (defined as the hydraulic diameter of the channel) and b is a high order slip coefficient, defined as $b = \frac{1}{2}l_c\frac{\frac{\partial^2 u_{ns}}{\partial y^2}}{\left|\frac{\partial u_{ns}}{\partial y}\right|}$; u_{ns} being the corresponding no-slip velocity field. The remaining part of the calculation is same as before, and hence is not repeated here for the sake of brevity. However, an interesting comparison between our semi-analytical solutions and the results presented by Chen and Weng [5], with regard to the Nusselt number predictions considering higher order slip/jump conditions, is presented in Fig. 5 to summarize our findings in this regard. For effective comparisons, we chose the following expression for the dimensionless channel height: $L^* = \frac{L}{Ral_c}$. In essence, variations in average *Nu* with L^* are presented in Fig. 5, corresponding to $Kn = 0.09$, as a representative case. An excellent agreement between the present solutions and the numerical solutions can be observed for this case of an extended slip model as well.

4. Conclusions

A boundary layer analysis has been presented in this work to assess the implications of the developing regime transport on natural convection slip flows in vertical microchannels. With the consideration of temperature-independent thermo-physical properties, the boundary layer equations are solved by following the integral approach over the slip flow regime. Interestingly, these results agree excellently with the corresponding full-scale simulation predictions obtained by solving the Navier–Stokes–Fourier equations with variable-property considerations. This possibly leads to the conclusion that to the level of the details intended to be obtained from the analysis, the variations of

thermo-physical properties with temperature play only a marginal role in determining the entrance length and local Nusselt number variations for natural convection in microchannels. Therefore, the present boundary layer formulation may be considered as an inexpensive yet reasonably accurate design basis for natural convection microchannel slip flows, instead of attempting for time-intensive full-scale numerical computations over a wide gamut of operating conditions.

References

[1] M. Gad-el-Hak, The fluid mechanics of microdevices – the freeman scholar lecture, J. Fluid Eng., ASME 121 (1999) 5–33.

[2] C.-K. Chen, H.C. Weng, Natural convection in a vertical microchannel, J. Heat Transfer 127 (2005) 1053–1056.

[3] L. Biswal, S.K. Som, S. Chakraborty, Effects of entrance region transport processes on free convection slip flow in vertical microchannels with isothermally heated walls, Int. J. Heat Mass Transfer 50 (2007) 1248–1254.

[4] O.M. Haddad, M.M. Abuzaid, M.A. Al-Nimr, Developing free-convection gas flow in a vertical open–ended microchannel filled with porous media, Numer. Heat Transfer A 48 (2005) 693–710.

[5] C.-K. Chen, H.C. Weng, Developing natural convection with thermal creep in a vertical microchannel, J. Phys. D: Appl. Phys. 39 (2006) 3107–3118.

[6] H.P. Kavehpour, M. Faghri, Y. Asako, Effects of compressibility and rarefaction on gaseous flows in microchannels, Numer. Heat Transfer A 32 (1997) 677–696.

[7] E.G.R. Eckert, R.M. Drake Jr., Analysis of Heat and Mass Transfer, McGraw-Hill, NY, 1972.